



# Estimation of lunar surface temperatures and thermophysical properties: test of a thermal model in preparation of the MERTIS experiment onboard BepiColombo

Karin E. Bauch <sup>a,\*</sup>, Harald Hiesinger <sup>a</sup>, Jörn Helbert <sup>b</sup>, Mark S. Robinson <sup>c</sup>, Frank Scholten <sup>b</sup>

<sup>a</sup> Institut für Planetologie, Westfälische Wilhelms-Universität Münster, Wilhelm-Klemm-Str. 10, 48149 Münster, Germany

<sup>b</sup> Institut für Planetenforschung, Deutsches Zentrum für Luft- und Raumfahrt (DLR), Rutherfordstr. 2, 12489 Berlin, Germany

<sup>c</sup> School of Earth and Space Exploration, Arizona State University, Tempe, AZ 85287, USA



## ARTICLE INFO

### Article history:

Received 27 July 2013

Received in revised form

10 April 2014

Accepted 7 June 2014

Available online 19 June 2014

### Keywords:

Moon

Mercury

MERTIS

Thermal model

## ABSTRACT

The Mercury Radiometer and Thermal Infrared Spectrometer (MERTIS) is part of the payload on the joint ESA-JAXA BepiColombo Mission, scheduled for launch in 2016. The spectrometer is designed to map surface compositions, to identify rock-forming minerals, to map surface mineralogy, and to study surface temperature variations. In preparation of the experiment we developed a thermal model that calculates surface temperatures based on appropriate insolation conditions and thermophysical properties. In the absence of thermal measurements on Mercury, we validate the model with lunar parameters. The results show good agreement with Apollo 17, Clementine and LRO-Diviner data. With appropriate changes of the orbital parameters and ephemeris data this model can be applied to the conditions of Mercury.

© 2014 Elsevier Ltd. All rights reserved.

## 1. Introduction

Part of the payload on the joint ESA-JAXA BepiColombo Mission, scheduled for launch in 2016, is the Mercury Radiometer and Thermal Infrared Spectrometer – MERTIS (Benkhoff et al., 2010; Hiesinger et al., 2010, 2014). MERTIS combines a push-broom IR grating spectrometer (TIS) with a radiometer (TIR), operating in the wavelength range of 7–14 μm and 7–40 μm, respectively, with a spatial resolution of 500 m globally and up to 280 m for 5–10% of the surface (Hiesinger et al., 2014). The spectrometer is designed to map surface compositions, to identify rock-forming minerals, to map surface mineralogy, and to study surface temperature variations (Hiesinger et al., 2010). Analysis of the temperature variations will provide information about the thermophysical properties of the regolith at the surface and in the upper subsurface layers. In preparation of the experiment we developed a thermal model that calculates surface temperatures based on temperature and depth-dependent thermal and physical properties of the regolith, e.g., the density, heat capacity, and thermal conductivity, as well as albedo and local topography. In the absence of thermal measurements on Mercury, we validate the model with lunar parameters. Here we investigate the temperature variations of the lunar surface and compare the results with

previous efforts of measuring lunar surface temperatures, which have been carried out from Earth-based observations (e.g., Pettit and Nicholson, 1927, 1930; Saari and Shorthill, 1972; Saari, 1964), spacecraft observations (Chan et al., 2010; Lawson et al., 2000; Paige et al., 2010b), and ground-based in situ measurements (Keihm and Langseth, 1973, 1975; Langseth et al., 1976a, 1976b).

Previous studies of the lunar surface have shown that thermal emission contributes to the observed signal from a surface and can influence the spectral characteristics in the thermal infrared (TIR), e.g., the depth of absorption bands (Clark, 2009; Pieters et al., 2009; Sunshine et al., 2009). This effect becomes evident at wavelengths longer than 2 μm on the Moon (Clark, 1979; Pieters et al., 2009) and approximately 1.5 μm on Mercury (Clark, 1979). Therefore, accurate knowledge of the thermal behavior of the surface is needed. The model used in this work solves the one-dimensional heat transfer equation, based on depth- and temperature-dependent thermophysical parameters, topography, and ephemeris data from the Jet Propulsion Laboratory (JPL) horizons software (Giorgini et al., 1996). This study provides new and updated research on the temperature behavior of the lunar surface, by taking into account the surface and subsurface thermal and physical properties, namely albedo, bulk density, heat capacity and thermal conductivity. These properties have been determined by in situ measurements on the lunar surface during the Apollo missions, analyses of returned samples from Luna and Apollo missions, and spacecraft observations (Cremers, 1973; Hemingway and Robie, 1973; Hemingway et al., 1973; Robie and Hemingway, 1971; Robie et al., 1970; Shkuratov and

\* Corresponding author. Tel.: +49 251 8339075; fax: +49 251 8336301.

E-mail address: [karin.bauch@uni-muenster.de](mailto:karin.bauch@uni-muenster.de) (K.E. Bauch).

Bondarenko, 2001). Previous efforts of measuring and modeling surface temperatures have been carried out from Earth-based observations (e.g., Pettit and Nicholson, 1927, 1930; Saari and Shorthill, 1972; Saari, 1964), in situ measurements (Keihm and Langseth, 1973; Langseth et al., 1976a), spacecraft observations (Chan et al., 2010; Lawson et al., 2000; Mendell, 1976a; Paige et al., 2010b), and also temperature models (Lawson et al., 2000; Linsky, 1966; Racca, 1995; Salvail and Fanale, 1994; Urquhart and Jakosky, 1997; Vasavada et al., 1999, 2012).

## 2. Previous temperature measurements

Lunar surface temperatures have been determined by Earth-based, spacecraft, and ground-based observations over the last decades (e.g., Langseth et al., 1976a, 1976b; Lawson et al., 2000; Paige et al., 2010a, 2010b; Pettit and Nicholson, 1927, 1930; Saari and Shorthill, 1972). Prior to spacecraft observations a number of Earth-based temperature measurements have been carried out (e.g., Low, 1965; Pettit and Nicholson, 1927, 1930). Such observations of nighttime temperatures are limited by the sensitiveness of the thermocouple circuit and area of receiver (Pettit and Nicholson, 1930). Thus temperatures of less than 100 K will be difficult to determine (Pettit and Nicholson, 1930). During the lunar day it is difficult to separate emitted and reflected radiation. Therefore, temperatures need to be extrapolated from measurements during eclipses (Cremers et al., 1971). At noon, temperatures between 374 K and 393 K have been measured. Temperatures at sunset were found to be between 170 K and 181 K, at sunrise 109 K, and at midnight around 120 K (Pettit and Nicholson, 1930).

During the Apollo missions several in situ temperature measurements were carried out (e.g., Langseth et al., 1972, 1976b). For the purpose of this study, the results of Apollo 17 are of major importance. This mission landed in the Taurus–Littrow valley, located in the southeast ring of Mare Serenitatis (Schmitt, 1973). One of the scientific experiments of the Apollo Lunar Surface Experiments Package (ALSEP) was a heat-flow experiment, which was designed to measure the thermal properties and thermal gradient within the lunar subsurface in order to determine the heat flux from the lunar interior (Langseth et al., 1976a). The variation of surface temperatures as a function of time at the Apollo 17 landing site is shown in Fig. 1 as derived by Keihm and Langseth (1973). Temperature varies more than 280 K during one lunar cycle between the maximum temperature of  $384 \pm 6$  K and pre-sunrise temperature of  $102 \pm 1.5$  K (Keihm and Langseth, 1973). Due to the lack of an atmosphere, rapid temperature changes occur at sunrise and sunset. The midnight temperature ( $106 \pm 2$  K) fits well with infrared observation of 104 K by Saari (1964).

In addition to the in situ experiment, this mission carried the Infrared Scanning Radiometer (ISR) onboard the Command-Service Module, which obtained thermal maps of 20–25% of the surface with a spectral band pass from 1.2  $\mu\text{m}$  to 70  $\mu\text{m}$  (Mendell and Low, 1975, 1974). Nighttime surface temperatures reveal the existence of thermal anomalies correlated to impact craters (Mendell, 1976b). Such temperature anomalies can be explained by blocky material, which stores more heat during the night than the surrounding fine-grained regolith (Mendell, 1976a).

The Deep Space Program Science Experiment (DSPSE), also known as Clementine mission was launched in 1994 and orbited the Moon between February 19 and May 3, 1994 (Nozette et al., 1994). The long-wavelength infrared (LWIR) camera measured surface emission between 8 and 9.5  $\mu\text{m}$  (Lucey et al., 2006). LWIR data have been analyzed in detail by Lawson et al. (2000). While in orbit for two lunar days, nadir looking images were obtained near local noon. Lawson et al. (2000) derived a global mosaic of

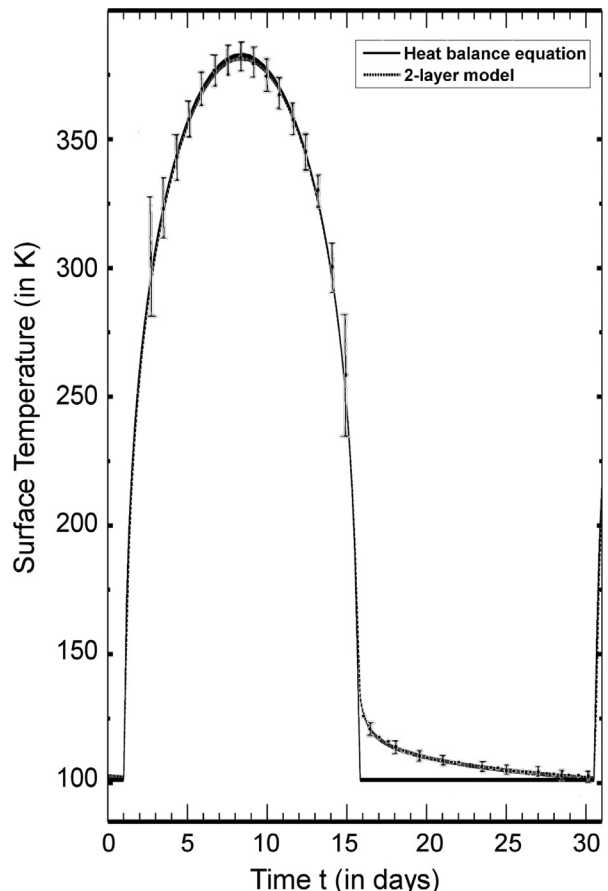


**Fig. 1.** Surface temperatures at Taurus–Littrow as a function of time. Temperature measurements (points and error bars) are taken from Keihm and Langseth (1973). The solid curve shows the solution of the heat balance at the surface, the dashed curve shows the solution of the 2-layer model as described above. Both models fit the daytime temperatures, however, the heat balance model fails in representing temperatures after sunset. Only the 2-layer model shows a good agreement with Apollo 17 data over the whole lunation.

image-averaged daytime temperatures with a resolution of  $1^\circ/\text{px}$  near local noon. Longitudinal gaps exist between orbital passes. Near local noon, surface temperatures vary about 200 K between equatorial and polar regions. Lawson et al. (2000) fitted LWIR temperatures by an eighth-order polynomial. The temperature difference between LWIR measured data and polynomial-fit highland temperatures has also been determined. Dark mare regions have temperatures up to 10 K warmer than highland terrain. High albedo features remain colder than the surrounding regions. The temperature differences are expected to be the result of albedo variations, rather than surface composition or thermal inertia (Lawson et al., 2000).

The Diviner Lunar Radiometer Experiment onboard NASA's Lunar Reconnaissance Orbiter (LRO) is mapping surface temperatures since July 2009. Temperatures are acquired at channel 6 (12.5–25  $\mu\text{m}$ ), channel 7 (25–41  $\mu\text{m}$ ), channel 8 (50–100  $\mu\text{m}$ ), and channel 9 (100–400  $\mu\text{m}$ ), and cover the whole range of temperature variations (Paige et al., 2010a; Vasavada et al., 2012). The spatial resolution is about 320 m along track and 160 m across track, from an altitude of 50 km (Vasavada et al., 2012) and is therefore appropriate to study both global and local temperature variations. Nighttime temperature observations confirm the existence of thermal anomalies associated with areas of high rock abundances, e.g., impact craters (Bandfield et al., 2011).

### 3. MERTIS—Mercury Radiometer and Thermal Infrared Spectrometer

The MERTIS instrument is designed for studying the surface composition and mineralogy of Mercury (Hiesinger et al., 2010). It combines an uncooled push broom grating IR-spectrometer (TIS) with a radiometer (TIR), covering the wavelength region of 7–14 μm and 7–40 μm, respectively (Hiesinger et al., 2010). The radiometer will measure both the day and nightside temperatures of Mercury at the same location that is observed by the spectrometer (Hiesinger et al., 2010). Observing the same spot with the TIS and TIR allows for cross-checks of surface temperature derivation between both methods (Hiesinger et al., 2010). Measuring Mercury's temperatures during the night will provide information about the thermophysical properties of the regolith. The instrument will obtain data from different regions and at different local times, but also measure temperatures for the same region at different local times in order to monitor the temperature variations during the night (Hiesinger et al., 2010).

## 4. Thermophysical surface and subsurface model

### 4.1. Heat conduction equation

The temperature variations of the lunar regolith can be calculated by solving the heat conduction equation (e.g., Cremers et al., 1971; Morrison, 1970; Urquhart and Jakosky, 1997). Determination of surface and subsurface temperatures of the Moon is a boundary value-initial condition problem in partial differential equations for a semi-infinite solid (Jones et al., 1975; Ulrichs and Campbell, 1969; Wesselink, 1948). Because investigated depths are small compared to the lunar radius, the curvature of the surface can be neglected (Wesselink, 1948). Lateral heat transfer can also be neglected, because the length scales for lateral heat transfer are larger than for vertical heat transfer (Salvail and Fanale, 1994). In this case, the problem can be reduced to one-dimensional heat conduction:

$$\rho(z)C(T)\frac{\partial T(z,t)}{\partial t} = \frac{\partial}{\partial z}\left[k(z,T)\frac{\partial T(z,t)}{\partial z}\right]. \quad (1)$$

The thermal parameters density ( $\rho$ ), heat capacity ( $C$ ) and thermal conductivity ( $k$ ) can vary with depth ( $z$ ) and/or temperature ( $T$ ). The boundary condition at the surface is given by the energy balance as

$$\epsilon\sigma T_0^4(t) = F(t) + k(z,T)\frac{\partial T(z,t)}{\partial z}|_{z=0}. \quad (2)$$

The first term of this energy balance equation represents the radiation loss into space. Heat loss by radiation is described by a fourth power law (Jaeger, 1953).  $\epsilon$  is the emissivity of the surface in comparison to a black body at the same temperature,  $\sigma$  is the Stefan–Boltzmann constant and  $T_0(t)$  is the surface temperature.  $F(t)$  represents the solar insolation and the last term represents the subsurface conduction. Solar insolation is a function of time and given by

$$F(t) = \frac{S_0}{R(t)^2} \cos(\theta(t))(1-A). \quad (3)$$

Solar heating is depending on the surface albedo ( $A$ ) and the orbital position of the Moon, which changes with time. It includes the distance to the Sun  $R(t)$ , the solar flux  $S_0$  at 1 AU and the solar incidence angle  $\theta(t)$ . The solar incidence angle is the angle between the direction to the Sun and a line normal to the surface. It varies with time and depends on the latitude, tilt, and azimuth of the local surface for which the temperature is calculated (e.g., Schorghofer and Edgett, 2006). Following Kimball and Hand

(1922) and Kimball (1925), the angle  $\theta$  of a sloping surface is calculated by

$$\cos \theta = \cos \nu \sin \alpha + \sin \nu \cos \alpha \sin(90 - \Delta\omega). \quad (4)$$

In this equation,  $\Delta\omega$  is the difference between the azimuth of the Sun and the aspect of the dipping surface,  $\nu$  is the angle between a horizontal and the sloping surface and  $\alpha$  is the solar altitude (Kimball and Hand, 1922; Kimball, 1925). When the Sun is below the local horizon Eq. (3) is reduced to  $F(t)=0$  and the surface boundary condition becomes

$$\epsilon\sigma T_0^4(t) = k(z,T)\frac{\partial T(z,t)}{\partial z}|_{z=0}. \quad (5)$$

The location and orientation of the Moon with respect to the Sun is derived from JPL Ephemeris Data for each time step (Giorgini et al., 1996). On the Moon there is no appreciable atmosphere to affect surface temperatures or contribute to the thermal conductivity (Morrison, 1970; Paige et al., 2010a).

The lower boundary condition is

$$q = -\lim_{z \rightarrow z_b} k(z,T)\frac{\partial T(z,t)}{\partial z}. \quad (6)$$

This equation implies that the daily downwelling heat flux approaches zero as  $z$  gets large and the upwelling heat flux approaches a constant geothermal flux  $q$  (Cremers et al., 1971; Keihm et al., 1973; Urquhart and Jakosky, 1997). Therefore  $z_b$  has to be deeper than the intrusion depth of any daily or annual temperature variations (Keihm et al., 1973). The probes at the Apollo 15 and 17 landing site show temperature variations of a 1 year period at all sensors at a depth of 120 cm below the surface (Langseth et al., 1976b). Therefore we chose a depth of  $z_b=2$  m. The calculation is based on variable space increments. The increments are of varying size with smallest increments close to the surface, where large temperature variations exist, and are increasing with increasing depths. Because there is no analytical solution for the set of equations, the use of a numerical model is required. The spatial discretization is based on a second-order accurate method of lines (Skeel and Berzins, 1990). Time integration is done using an implicit time integration code with quasi-constant step size as described in detail by Shampine and Reichelt (1997).

### 4.2. Thermophysical parameters

Thermal and physical properties of the upper subsurface layers strongly influence the thermal behavior of the lunar surface (Lawson et al., 2000; Racca, 1995; Urquhart and Jakosky, 1997). The brecciated and fragmented surface forms the regolith which highly insulates the surface (e.g., Racca, 1995). Knowledge of the thermal properties of the regolith has been obtained from ground-based and spacecraft observations, in situ measurements and laboratory studies of returned samples as reviewed by Vasavada et al. (1999). In the following sections we describe several parameters that influence the thermal properties and hence have been considered in our model, including heat capacity, bulk density, and thermal conductivity.

#### 4.2.1. Heat capacity

Heat capacity of the lunar regolith has been determined for different samples returned by the Apollo 11, 12, 14, 15 and 16 missions (Hemingway and Robie, 1973; Hemingway et al., 1973; Robie and Hemingway, 1971; Robie et al., 1970). The Apollo 11 samples include fine-grained vesicular basalt (sample 10057), breccia (10021), and soil (10084). Apollo 12 sample is an olivine dolerite (12018), which is a crystalline rock. Apollo 14 samples include soil (14163) and breccia (14321), Apollo 15 samples soil (15301) and basalt (15555), and Apollo 16 is a soil sample (60601).

In the studies mentioned above, heat capacity was measured using adiabatic calorimeters in the range between 90 K and 350 K. The best fit to all the data was obtained by using a fourth-degree polynomial (Hemingway et al., 1973)

$$C(T) = -2.3173 \times 10^{-2} + 2.1270 \times 10^{-3} T + 1.5009 \times 10^{-5} T^2 - 7.3699 \times 10^{-8} T^3 + 9.6552 \times 10^{-11} T^4. \quad (7)$$

Within the range of lunar equatorial surface temperatures, Eq. (7) represents the experimental data to better than 10% (Hemingway et al., 1973).

#### 4.2.2. Bulk density

Based on Arecibo radar data Shkuratov and Bondarenko (2001) found regolith thicknesses of 5 m and 12 m for mare regions and highlands, respectively. Thin regolith thicknesses of 4 m cover Mare Serenitatis, Mare Tranquillitatis and Mare Humorum. These estimates imply that the transition to underlying bedrock does not have to be incorporated in the model on a large scale. Instead it can be assumed that the density increases with depth solely due to compaction of particles (Jones, 1968). At the surface the density varies between 800 kg/m<sup>3</sup> at the Luna 13 landing site and 1500–1700 kg/m<sup>3</sup> for the Luna 16 landing site (summarized by Carrier et al., 1991).

Similar to the models of Mitchell and de Pater (1994) and Vasavada et al. (1999), we assume that the regolith consists of two layers with increasing density. The upper layer (< 2 cm) has a density of  $\rho_{\text{top}}=1300 \text{ kg/m}^3$ , while the bottom layer is composed of more dense material with  $\rho_{\text{bot}}=1800 \text{ kg/m}^3$ .

#### 4.2.3. Thermal conductivity

Porous material under vacuum conditions such as the lunar or hermean regolith transfers heat in two different ways: the first is solid conduction through particles and across interparticle contacts and the second is radiation across void spaces (Cremers, 1973)

$$k = k_s + k_r \quad (8)$$

with the solid conduction  $k_s$  and radiative term  $k_r$ . Determination of both terms using lunar fines is challenging, because only few grams were available (Cremers, 1973). Studies of dry rock powders indicate that thermal conductivities strongly depend on temperature, because a fraction of energy is transported by radiation between grains (Ulrichs and Campbell, 1969; Wechsler and Simmons, 1966). The radiative term increases with temperature cubed, therefore it can be written as

$$k = a_0 + a_3 T^3. \quad (9)$$

Coefficients  $a_0$  and  $a_3$  have been derived from different studies, summarized in Table 1. In addition, analyses of Apollo sample 12001 for different densities reveals that thermal conductivity is not only a function of temperature, but also density (Cremers, 1973). This behavior was also described by Fountain and West (1970) and Jones et al. (1975), who confirmed that thermal conductivity is a function of density and therefore depth.

**Table 1**

Coefficients  $a_0$  and  $a_3$  for thermal conductivity for Apollo sample 12001 measured under different densities (Cremers, 1973).

Density kg/m <sup>3</sup>	$a_0$ $10^{-3} \text{ W/m K}$	$a_3$ $10^{-11} \text{ W/m K}^4$
1300	0.922	3.19
1640	0.985	2.06
1970	1.25	1.59

Fig. 2 shows the variation of thermal conductivities for Apollo sample 12001 for different densities (Table 1). In the range of lunar surface temperatures, thermal conductivity varies by a factor of three for a low density of 1300 kg/m<sup>3</sup>. Sample 12001 shows that at high temperatures, conductivity at low densities is highest. The lower density arises from a higher porosity and indicates a higher degree of radiative heat transfer (Cremers, 1973). Denser material has a higher conductivity at low temperatures, when heat is primarily transported by solid conduction.

At the Apollo 17 landing site in situ measurements show that there is a sharp increase in thermal conductivity at a depth of about 2 cm (Kiefer, 2012). In this study we use the effective thermal conductivity described by Mitchell and de Pater (1994), who included radiative heat transfer between grains as

$$k(T) = k_c [1 + X(T/350)^3]. \quad (10)$$

In this equation  $k_c$  describes the phonon conductivity and  $X$  the ratio of radiative to solid conduction. Both parameters are assumed to vary with depth (Mitchell and de Pater, 1994), therefore Vasavada et al. (1999) chose  $X_{\text{top}}=1.48$  for the upper 2 cm and  $X_{\text{bot}}=0.073$  for the underlying layer. The lower value of  $X_{\text{bot}}$  corresponds to the larger solid conduction. For the top layer  $k_c \text{ top}=9.22 \times 10^{-4} \text{ W/m K}$  and the bottom layer  $k_c \text{ bot}=9.3 \times 10^{-3} \text{ W/m K}$  were chosen (Vasavada et al., 1999).

## 5. Results

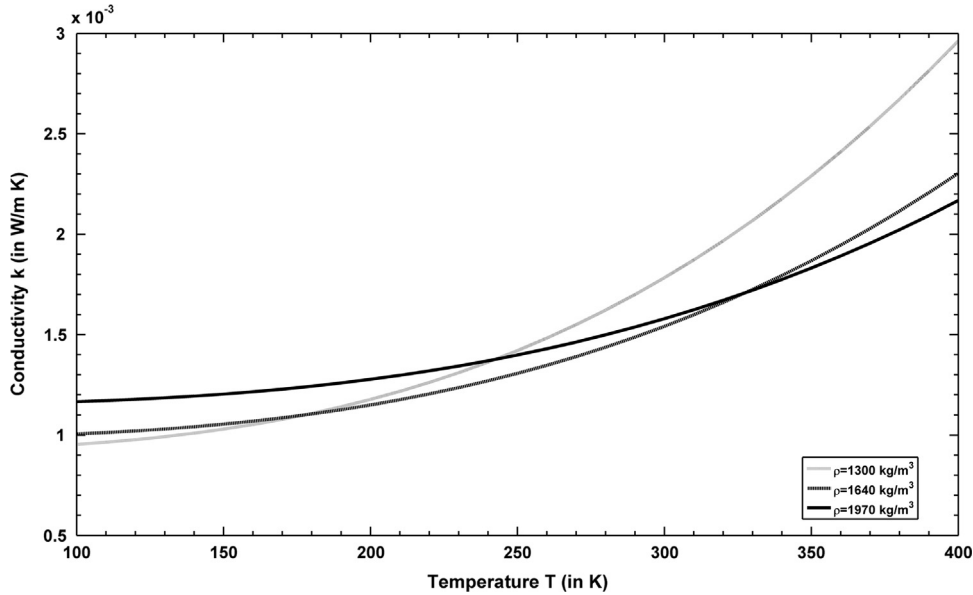
### 5.1. Model temperatures at the Apollo 17 landing site

Fig. 1 shows the Apollo 17 temperature measurements (Keihm and Langseth, 1973) compared to our model results (dashed line) for an average albedo of 0.12 and the heat balance equation (solid line) as a function of time. Ephemeris data were computed with time steps of 4 h. Both models fit the daytime temperatures well, however, only the 2-layer model (dashed line) shows a good agreement with Apollo 17 data over the entire lunation. At sunrise and sunset both models show very fast temperature changes. The maximum modeled temperature is 381.2 K, while the maximum measured temperature is  $384 \pm 6 \text{ K}$  (Keihm and Langseth, 1973). The modeled pre-sunrise temperature of 103.2 K also fits the measured temperature of  $102 \pm 1.5 \text{ K}$  (Keihm and Langseth, 1973).

Theoretical calculations of temperatures over large timescales (Fig. 3) reveal a periodicity not included in the Apollo temperature measurements. The amplitude of the maximum surface temperatures varies between about 372 K and 381 K over the course of an 18.6 year period. This variation corresponds to the precession of the lunar orbit. This precession modifies the maximum solar zenith angle, which directly influences maximum surface temperatures (Wieczorek and Huang, 2006). As mentioned above, this periodicity has been neglected in the calculations of Apollo 15 and 17 temperatures, which cover only a period of 3.5 and 2 years, respectively (Wieczorek and Huang, 2006). Therefore the reliability of the measured heat flow remains unclear (Wieczorek and Huang, 2006).

### 5.2. Global brightness temperature

The investigation of surface temperatures utilizes the Clementine UVVIS 750 nm albedo map with a resolution of  $\sim 0.4^\circ$  per pixel as input to Eq. (5). This resolution corresponds to 12.5 km per pixel at the equator. We run the model over a period of 1 year, covering the time span of Clementine observations (Nozette et al., 1994). In our global model the surface is assumed to be flat, without any topography. Latitudes higher than  $75^\circ$  were excluded from this study, because topographic effects can heavily influence



**Fig. 2.** Thermal conductivity as a function of temperature and density for Apollo 12 sample 12001. Parameters are described in Table 1. Conductivity has been measured for different densities by Cremers (1973).

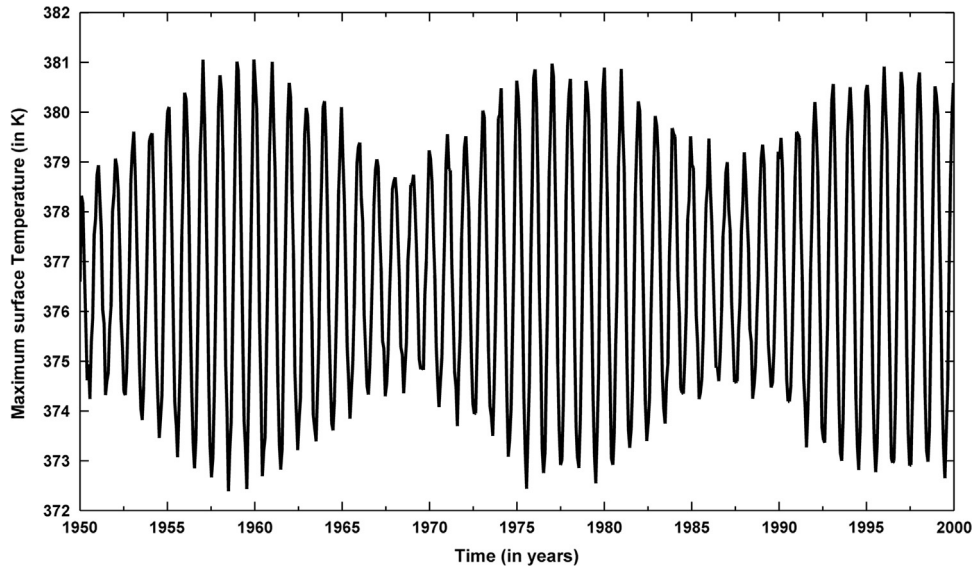


**Fig. 3.** Estimated maximum surface model temperatures as a function of time at the Apollo 17 landing site between 1950 and 2000. Amplitudes vary about 9 K, following an 18.6 year period.

the temperatures (Lawson et al., 2000). Variations of surface brightness temperatures are assumed to be only controlled by albedo, angle of solar incidence, and the thermal properties described above. The thermal parameters are assumed to be uniform over the lunar surface.

We find that during daytime dark mare regions are warmer than highland terrains at the same latitude. Shortly after sunrise the surface already reaches temperatures of more than 270 K for latitudes between 30° north and south (Fig. 4a). Before sunset, mare surfaces are warmer at the same incidence angle due to the heat stored in the subsurface (Fig. 4c). The temperatures clearly reflect the brightness of the surface and margins of mare and highland regions become visible in the temperature map.

The maximum surface temperatures for latitudes between 75° north and 75° south are shown in Fig. 4b. At high latitudes, maximum surface temperatures reach 240 K and about 390 K within mare regions near the equator. Nighttime temperatures

are around 100 K, which is in good agreement with the Apollo 15 and 17 measurements described by Keihm and Langseth (1973). High albedo features, such as crater Copernicus (10° N, 340° E) are significantly colder than the surrounding mare.

At high latitudes, brightness differences are not clearly visible in the temperature map. For example the South Pole Aitken basin (centered at 56°S, 180° E) is a low albedo region on the southern farside (Pieters et al., 2001), but is only about 6 K warmer than the surrounding. In order to better analyze the influence of albedo on global surface temperatures, we derived a map that shows the difference between our model temperatures based on albedo minus model temperatures of an assumed uniformly bright surface with an albedo of 0.12 (Fig. 4d). Maximum temperatures differ about  $\pm 15$  K between mare regions and highlands. Few very bright surfaces have even lower temperatures.

On a global scale, temperatures near local noon have been measured by the Clementine long-wave infrared (LWIR) camera

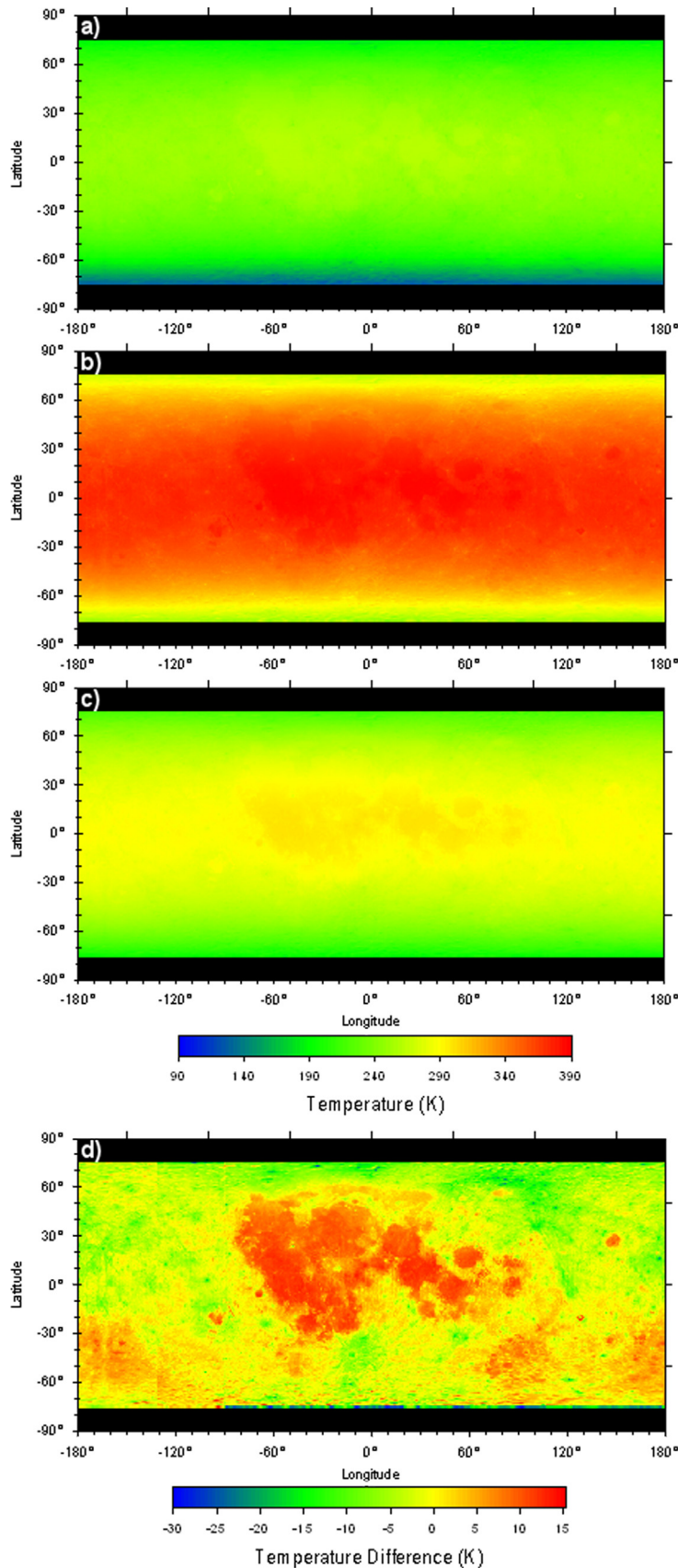


**Fig. 4.** Surface brightness temperatures between 75° north and south. (a) 1 day after local sunrise, (b) at local noon, (c) 1 day before local sunset, (d) temperature difference between model temperatures at local noon and model temperatures of a surface with a uniform albedo of 0.12.

and were analyzed by [Lawson et al. \(2000\)](#). Their map has a resolution of  $1^\circ/\text{px}$ . Our modeled temperatures show a good agreement with the measured data. Near the equator, the Moon is about 100 K warmer than towards the poles. In addition, brightness of the soil influences surface temperatures. The difference map of this study shows differences slightly larger than for measured data. Due to the better resolution, some bright features show up with high temperature differences that are not visible in Clementine measurements. Moreover margins of mare are more clearly defined.

### 5.3. Slope effects on surface temperatures

The lunar surface is not a perfect sphere as assumed for our calculation of surface temperatures on a global scale. The terminator, which is the transition between day and night, is not a sharp line, but is influenced by topographic features. Shadowing of a surface may be caused by topography features in the direct line to the Sun. Consequently, after sunset, high standing areas and crater walls will still receive sunlight, while surrounding low-lying flat areas are already dark. Some impact craters near the lunar poles remain in permanent shadow, while their crater walls may receive sunlight over almost the entire lunation ([Bussey et al., 1999](#)). In addition, the insolation angle may vary when observing a sloping surface ([Kimball and Hand, 1922](#); [Kimball, 1925](#); [Schorghofer and Edgett, 2006](#)) and therefore influence the surface temperatures at all times of the lunar day. Temperature calculations of the lunar surface, when investigated on a smaller scale, should therefore take into account the surface's topography, especially in the form of slopes. Due to topography, an observed surface emits radiation to other visible surface facets. However, at the same time the observed surface also receives scattered energy from neighboring surfaces ([Vasavada et al., 1999](#)). This effect is similar to the reflectance of incident sunlight, which can be reflected from one surface to neighboring surfaces. Temperatures of sloping surfaces are a function of both the dip angle and azimuth ([Keihm, 1984](#); [Schorghofer and Edgett, 2006](#); [Siegler et al., 2011](#)).

For our study we use topography data (DEM) for the Taurus-Littrow valley, obtained from Lunar Reconnaissance Orbiter Camera (LROC) Wide Angle Camera (WAC) images ([Fig. 5a](#)) with a resolution of  $100 \text{ m}/\text{px}$  ([Scholten et al., 2012](#)). At Taurus-Littrow, elevations range from about  $-4 \text{ km}$  to  $\sim 0.8 \text{ km}$ , with maximum slopes of about  $10^\circ$ .

The surface temperatures about 1 day after local sunrise are shown in [Fig. 5b](#). South-east facing slopes already have temperatures about 70 K higher than the flat surface where the Apollo module landed. Small craters are also clearly visible because of high temperature differences on the crater walls. Slopes facing away from the Sun have temperatures about 50 K lower than the flat surface of the landing site. At local noon ([Fig. 5c](#)), maximum temperatures are 380 K with differences on the order of 25 K. South facing slopes are slightly warmer than the flat surface on the valley floor. Close to sunset, the temperature variation is similar to sunrise temperatures, with warm surfaces facing in south-west direction.

A comparison of temperatures of the flat valley floor to those of sloping surfaces shows that surface temperatures under low solar elevation angles are mainly controlled by slopes and that albedo has little influence. Near local noon both effects control the temperatures. At latitudes closer to the equator, and therefore higher solar elevation angles at local noon, temperatures are mainly governed by surface brightness. However, at higher latitudes and low solar elevation angles, surface topography has a major influence.

## 6. Summary

We have developed a thermal model to calculate temperatures of airless planetary surfaces by taking into account the temperature- and depth-dependent thermophysical properties, radiation loss into space, subsurface conduction, and solar insolation. This model has been tested using parameters of the lunar regolith. The model can also be applied to study the temperature variations of the surface of Mercury, once MERTIS will provide detailed data. The surface of Mercury is assumed to be thermally similar ([Vasavada et al., 1999](#)), with porous surface layers and areas of higher thermal inertia, due to, for example impact craters. On the Moon, thermophysical parameters have been determined by in situ measurements on the surface, returned samples, and spacecraft and ground-based observations. Radiation loss is depending on the surface's emissivity and surface temperature. Subsurface cooling is controlled by the thermal inertia, especially thermal conductivity, which depends on temperature and depth. Heating of a surface strongly depends on the brightness, but also the topography, especially in the form of slopes that change the solar insolation angle.

A comparison to Apollo 17 data shows good agreement between measured surface temperatures ([Keihm and Langseth, 1973](#)) and model temperatures derived from our thermal model ([Fig. 1](#)). The subsurface that gives the best-fit to the data includes a layered regolith, where the regolith becomes denser and more conductive with increasing depth ([Kiefer, 2012](#); [Vasavada et al., 1999](#)). At low temperatures, heat is mainly transferred by solid conduction between the particles, while radiation dominates at high temperatures ([Fig. 2](#)). Long-term analysis reveals a periodicity of maximum surface temperatures within a period of 18.6 years ([Fig. 3](#)). This variation is caused by the precession of the lunar orbit and has been included in our model when calculating surface temperatures for various times.

Global temperatures at local noon vary between 390 K near the equator and 240 K at latitude  $75^\circ$  ([Fig. 4b](#)). Dark mare regions have significantly higher surface temperatures than bright areas. Shortly after sunrise temperatures in equatorial regions reach temperatures  $> 270 \text{ K}$  ([Fig. 4a](#)). The temperature maps obtained in this study have a resolution of  $0.4^\circ/\text{px}$ , corresponding to  $12.5 \text{ km}$  at the equator.

Depending on their orientation, sloping surfaces can increase or decrease the surface temperatures due to the changes in solar incidence angle ([Fig. 5](#)). Very steep slopes at the limb can reach similar temperatures as a flat surface at high solar elevation angles. Brightness has an effect on temperatures at high elevation angles near local noon. Especially at low solar elevation angles the temperatures are strongly influenced by topography, which is particularly important for polar areas.

### 6.1. Implications for MERTIS

The study shows a good agreement of our model temperatures with different studies of measured lunar surface temperatures. The surface properties of Mercury and the Moon are assumed to be thermally similar ([Vasavada et al., 1999](#)) and there is no contribution of an atmosphere that needs to be considered in the thermal model (e.g., [Morrison, 1970](#)). Erosion is limited to impact cratering, which excavates rocks and pulverizes the surface material, hence having influence on the thermal properties (see [Fig. 2](#)). Therefore (with appropriate changes) it is possible to apply our model to the surface of Mercury. For example, the orbital parameters and ephemeris data need to be changed to Mercury. As soon as sufficient topography data is available, it is possible to model global temperature curves for all times of the hermean day. This study will become necessary in preparation of the MERTIS experiment onboard BepiColombo.

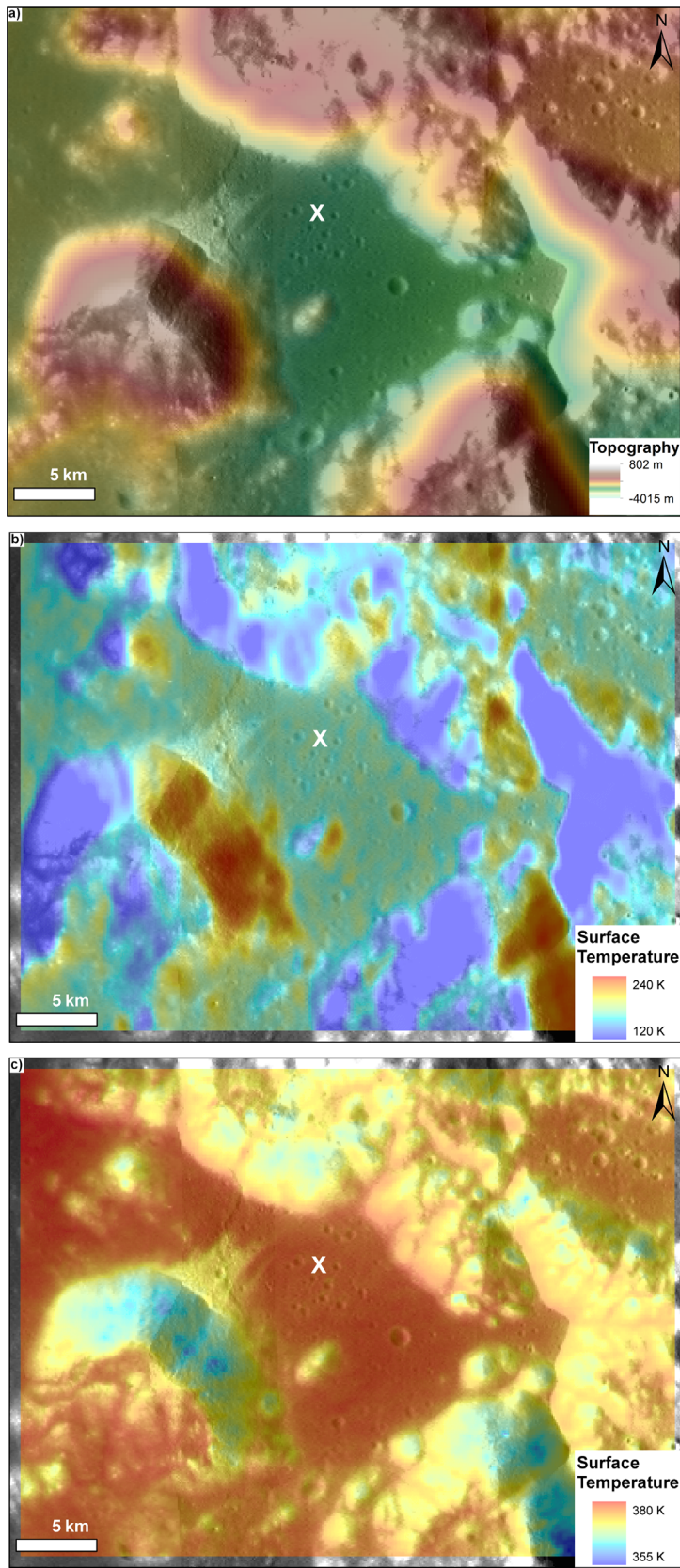


**Fig. 5.** (a) Topography of the Taurus–Littrow region determined from LROC-WAC images (Scholten et al., 2012). Elevation ranges from about  $-4$  km to  $0.8$  km, with slopes up to  $\sim 10^\circ$ . (b) Model surface temperatures shortly after sunrise, and (c) near local noon. All images are centered at  $20.09^\circ\text{N}$  and  $30.83^\circ\text{E}$ , white X marks the Apollo 17 landing site.

## Acknowledgments

We thank Dennis Reiss for generating the albedo maps used in this study. We appreciate the constructive and helpful comments and suggestions provided by Matt Siegler, which greatly improved the manuscript. Funding for this study was provided by the German Space Agency (DLR), which supported the MERTIS projects 50 QW 0901 and 50 QW 1302 in the framework of the BepiColombo mission.

## References

- Bandfield, J.L., Ghent, R.R., Vasavada, A.R., Paige, D.A., Lawrence, S.J., Robinson, M.S., 2011. Lunar surface rock abundance and regolith fines temperatures derived from LRO Diviner Radiometer data. *J. Geophys. Res.* 116, E00H02.
- Benkhoff, J., van Casteren, J., Hayakawa, H., Fujimoto, M., Laakso, H., Novara, M., Ferri, P., Middleton, H.R., Ziethe, R., 2010. BepiColombo—Comprehensive exploration of Mercury: Mission overview and science goals. *Planet. Space Sci.* 58, 2–20.
- Bussey, D.B.J., Spudis, P.D., Robinson, M.S., 1999. Illumination conditions at the lunar south pole. *Geophys. Res. Lett.* 26, 1187–1190.
- Carrier, W.D., Olhoeft, G.R., Mendell, W.W., 1991. Physical properties of the lunar surface. In: Heiken, G., Vaniman, D., French, B.M. (Eds.), *Lunar Source Book—A User Guide to the Moon*. Cambridge University Press, New York, pp. 475–594.
- Chan, K.L., Tsang, K.T., Kong, B., Zheng, Y.-C., 2010. Lunar regolith thermal behavior revealed by Chang'E-1 microwave brightness temperature data. *Earth Planet. Sci. Lett.* 295, 287–291.
- Clark, R.N., 1979. Planetary Reflectance Measurements in the region of Planetary Thermal Emission. *Icarus* 40, 94–103.
- Clark, R.N., 2009. Detection of adsorbed water and hydroxyl on the Moon. *Science* 326, 562–564.
- Cremers, C.J., 1973. Thermophysical Properties of Apollo 12 Fines. *Icarus* 18, 294–303.
- Cremers, C.J., Birkebak, R.C., White, J.E., 1971. Lunar Surface Temperatures from Apollo 12. *Moon* 3, 346–351.
- Fountain, J.A., West, E.A., 1970. Thermal conductivity of particulate basalt as a function of density in simulated lunar and Martian environments. *J. Geophys. Res.* 75, 4063–4069.
- Giorgini, J.D., Yeomans, D.K., Chamberlin, A.B., Chodas, P.W., Jacobson, R.A., Keesey, M.S., Lieske, J.H., Ostro, S.J., Standish, E.M., Wimberly, R.N., 1996. JPL's On-Line Solar System Data Service. *Bull. Am. Astron. Soc.* 28, 1158.
- Hemingway, B.S., Robie, R.A., 1973. Specific heats of lunar Basalt, 15555, and Soils 15301 and 60601 from 90 to 350 K. Abstracts of Lunar and Planetary Science Conference. vol. no. 4, pp. 355–356.
- Hemingway, B.S., Robie, R.A., Wilson, W.H., 1973. Specific heats of lunar soils, basalt, and breccias from the Apollo 14, 15, and 16 landing sites, between 90 and 350 K. In: Proceedings of the Lunar Science Conference. vol. 4, pp. 2481–2487.
- Hiesinger, H., Helbert, J., Peter, G., Walter, I., D'Amore, M., Säuberlich, T., Weber, I., 2014. The Mercury thermal radiometer and thermal infrared spectrometer (MERTIS) for BepiColombo: a status report. *Lunar and Planetary Science Conference*. vol. 45, 1912.
- Hiesinger, H., Helbert, J., Team, M.C.-I., 2010. The Mercury Radiometer and Thermal Infrared Spectrometer (MERTIS) for the BepiColombo mission. *Planet. Space Sci.* 58, 144–165.
- Jaeger, J.C., 1953. The Surface Temperature of the Moon. *Aust. J. Phys.* 6, 10–21.
- Jones, B.P., 1968. Density-Depth Model for the Lunar Outermost Layer. *J. Geophys. Res.* 73, 7631–7635.
- Jones, W.P., Watkins, J.R., Calvert, T.A., 1975. Temperatures and thermophysical properties of the lunar outermost layer. *Moon* 13, 475–494.
- Keihm, S.J., 1984. Interpretation of the Lunar Microwave Brightness Temperature Spectrum: Feasibility of Orbital Heat Flow Mapping. *Icarus* 60, 568–589.
- Keihm, S.J., Langseth, M.G., 1973. Surface brightness temperatures at the Apollo 17 heat flow site: thermal conductivity of the upper 15 cm of regolith. In: Proceedings of the Lunar Science Conference. 4, pp. 2503–2513.
- Keihm, S.J., Langseth, M.G., 1975. Lunar microwave brightness temperature observations reevaluated in the light of Apollo program findings. *Icarus* 24, 211–230.
- Keihm, S.J., Peters, K., Langseth, M.G., Chute, J.L., 1973. Apollo 15 measurement of lunar surface brightness temperatures thermal conductivity of the upper 1 1/2 meters of regolith. *Earth Planet. Sci. Lett.* 19, 337–351.
- Kiefer, W.S., 2012. Lunar heat flow experiments: Science objectives and a strategy for minimizing the effects of lander-induced perturbations. *Planet. Space Sci.* 60, 155–165.
- Kimball, H.H., 1925. Daylight illumination on a Sloping Surface: a Correction. *Mon. Weather Rev.* 53, 448.
- Kimball, H.H., Hand, I.F., 1922. Daylight Illumination on Horizontal, Vertical, and Sloping Surfaces. *Mon. Weather Rev.* 50, 615–628.
- Langseth, M.G., Clark, S.P., Chute, J.L., Keihm, S.J., Wechsler, A.E., 1972. The Apollo 15 lunar heat-flow measurement. *Moon* 4, 390–410.
- Langseth, M.G., Keihm, S.J., Peters, K., 1976a. The revised lunar heat flow values. *Lunar and Planetary Science Conference*. 7, pp. 474–475.
- Langseth, M.G., Keihm, S.J., Peters, K., 1976b. Revised lunar heat-flow values. In: Proceedings of the Lunar Science Conference. 7, pp. 3143–3171.
- Lawson, S.L., Jakosky, B.M., Park, H.-S., Mellon, M.T., 2000. Brightness temperatures of the lunar surface: Calibration and global analysis of the Clementine long-wave infrared camera data. *J. Geophys. Res.* 105, 4273–4290.
- Linsky, J.L., 1966. Models of the lunar surface including temperature-dependent thermal properties. *Icarus* 5, 606–634.
- Low, F.J., 1965. Lunar Nighttime Temperatures Measured at 20 Microns. *Astrophys. J.* 142, 806–808.
- Lucey, P., Korotev, R.L., Gillis, J.J., Taylor, L.A., Lawrence, D., Campbell, B.A., Elphic, R., Feldman, B., Hood, L.L., Hunten, D., Mendillo, M., Noble, S., Papike, J.J., Reedy, R.C., Lawson, S.L., Prettyman, T., Gasnault, O., Maurice, S., 2006. Understanding the Lunar Surface and Space-Moon Interactions. *Rev. Mineral. Geochemistry* 60, 83–219.
- Mendell, W.W., 1976a. Degradation of large, period II lunar craters. In: *Proceedings of the Lunar Science Conference*. 7, pp. 2705–2716.
- Mendell, W.W., 1976b. Crater Degradation and Thermal Patterns. *Abstracts of Lunar Planetary Science Conference*. 7, pp. 552–554.
- Mendell, W.W., Low, F.J., 1974. Preliminary results of the Apollo 17 infrared scanning radiometer. *Moon* 9, 97–103.
- Mendell, W.W., Low, F.J., 1975. Infrared orbital mapping of lunar features. In: *Proceedings of the Lunar Science Conference*. 3, pp. 2711–2719.
- Mitchell, D.L., de Pater, I., 1994. Microwave Imaging of Mercury's Thermal Emission at Wavelengths from 0.3 cm to 20.5 cm. *Icarus* 110, 2–32.
- Morrison, D., 1970. Thermophysics of the planet Mercury. *Space Sci. Rev.* 11, 271–307.
- Nozette, S., Rustan, P., Pleasance, L.P., Kordas, J.F., Lewis, I.T., Park, H.S., Priest, R.E., Horan, D.M., Regeon, P., Lichtenberg, C.L., Shoemaker, E.M., Eliason, E.M., McEwen, A.S., Robinson, M.S., Spudis, P.D., Acton, C.H., Buratti, B.J., Duxbury, T.C., Baker, D.N., Jakosky, B.M., Blamont, J.E., Corson, M.P., Resnick, J.H., Rollins, C.J., Davies, M.E., Lucey, P.G., Malaret, E., Massie, M.A., Pieters, C.M., Reisse, R.A., Simpson, R.A., Smith, D.E., Sorenson, T.C., Breugge, R.W., Zuber, M.T., 1994. The clementine mission to the moon: scientific overview. *Science* 266, 1835–1839.
- Paige, D.A., Foote, M.C., Greenhagen, B.T., Schofield, J.T., Calcutt, S., Vasavada, A.R., Preston, D.J., Taylor, F.W., Allen, C.C., Snook, K.J., Jakosky, B.M., Murray, B.C., Soderblom, L.A., Jau, B., Loring, S., Bulharowski, J., Bowles, N.E., Thomas, I.R., Sullivan, M.T., Avis, C., Jong, E.M., Hartford, W., McCleese, D.J., 2010a. The Lunar Reconnaissance Orbiter Diviner Lunar Radiometer Experiment. *Space Sci. Rev.* 150, 125–160.
- Paige, D.A., Siegler, M.A., Zhang, J.A., Hayne, P.O., Foote, E.J., Bennett, K.A., Vasavada, A.R., Greenhagen, B.T., Schofield, J.T., McCleese, D.J., Foote, M.C., DeJong, E., Bills, B.G., Hartford, W., Murray, B.C., Allen, C.C., Snook, K., Soderblom, L.A., Calcutt, S., Taylor, F.W., Bowles, N.E., Bandfield, J.L., Elphic, R., Ghent, R., Glotch, T.D., Wyatt, M.B., Lucey, P.G., 2010b. Diviner Lunar Radiometer Observations of Cold Traps in the Moon's South Polar Region. *Science* 330, 479–482.
- Pettit, E., Nicholson, S.B., 1927. Temperature of the Dark Side of the Moon and of the Moon During Eclipse. *Publ. Astron. Soc. Pacif.* 39, 227–228.
- Pettit, E., Nicholson, S.B., 1930. Lunar radiation and temperatures. *Astrophys. J.* 71, 102–135.
- Pieters, C.M., Goswami, J.N., Clark, R.N., Annadurai, M., Boardman, J., Buratti, B., Combe, J.-P., Dyar, M.D., Green, R., Head, J.W., Hibbitts, C., Hicks, M., Isaacson, P., Klima, R., Kramer, G., Kumar, S., Livo, E., Lundein, S., Malaret, E., McCord, T., Mustard, J., Nettles, J., Petro, N., Runyon, C., Staid, M., Sunshine, J.M., Taylor, L.A., Tompkins, S., Varanasi, P., 2009. Character and spatial distribution of OH/H<sub>2</sub>O on the surface of the Moon seen by M3 on Chandrayaan-1. *Science* 326, 568–572.
- Pieters, C.M., Head, J.W., Gaddis, L., Jolliff, B., Duke, M., 2001. Rock types of South Pole-Aitken basin and extent of basaltic volcanism. *J. Geophys. Res.* 106, 28001–28022.
- Racca, G.D., 1995. Moon surface thermal characteristics for moon orbiting space-craft thermal analysis. *Planet. Space Sci.* 43, 835–842.
- Robie, R.A., Hemingway, B.S., 1971. Specific heats of the lunar breccia (10021) and olivine dolerite (12018) between 90 to 350 K. In: *Proceedings of the Lunar Science Conference* 2, pp. 2361–2365.
- Robie, R.A., Hemingway, B.S., Wilson, W.H., 1970. Specific heats of lunar surface materials from 90 to 350 K. In: *Proceedings of the Apollo 11 Lunar Science Conference*. 3, pp. 2361–2367.
- Saari, J.M., 1964. The surface temperature of the antisolar point of the Moon. *Icarus* 3, 161–163.
- Saari, J.M., Shorthill, R.W., 1972. The sunlit lunar surface. *Moon* 5, 161–178.
- Salvail, J.R., Fanale, F.P., 1994. Near-Surface Ice on Mercury and the Moon: A Topographic Thermal Model. *Icarus* 111, 441–455.
- Schmitt, H.H., 1973. Apollo 17 Report on the Valley of Taurus-Littrow. *Science* 182, 681–690.
- Scholten, F., Oberst, J., Matz, K.-D., Roatsch, T., Wählisch, M., Speyerer, E.J., Robinson, M.S., 2012. GLD100: The near-global lunar 100 m raster DTM from LROC WAC stereo image data. *J. Geophys. Res.* 117, E00H17.
- Schorghofer, N., Edgett, K., 2006. Seasonal surface frost at low latitudes on Mars. *Icarus* 180, 321–334.
- Shampine, L.F., Reichelt, M.W., 1997. The MATLAB ODE Suite. *SIAM J. Sci. Comput.* 18, 1–22.
- Shkurov, Y.G., Bondarenko, N.V., 2001. Regolith Layer Thickness Mapping of the Moon by Radar and Optical Data. *Icarus* 149, 329–338.
- Siegler, M.A., Bills, B.G., Paige, D.A., 2011. Effects of orbital evolution on lunar ice stability. *J. Geophys. Res.* 116, E03010.
- Skeel, R.D., Berzins, M., 1990. A method for the spatial discretization of parabolic equations in one space variable. *SIAM J. Sci. Stat. Comput.* 11, 1–32.

- Sunshine, J.M., Farnham, T.L., Feaga, L.M., Groussin, O., Merlin, F., Milliken, R.E., A'Hearn, M.F., 2009. Temporal and Spatial Variability of Lunar Hydration As Observed by the Deep Impact Spacecraft. *Science* 326, 565–568.
- Ulrichs, J., Campbell, M.J., 1969. Radiative heat transfer in the lunar and mercurian surfaces. *Icarus* 11, 180–188.
- Urquhart, M.L., Jakosky, B.M., 1997. Lunar thermal emission and remote determination of surface properties. *J. Geophys. Res.* 102, 10959–10969.
- Vasavada, A.R., Bandfield, J.L., Greenhagen, B.T., Hayne, P.O., Siegler, M.A., Williams, J.-P., Paige, D.A., 2012. Lunar equatorial surface temperatures and regolith properties from the Diviner Lunar Radiometer Experiment. *J. Geophys. Res.* 117, E00H18.
- Vasavada, A.R., Paige, D.A., Wood, S.E., 1999. Near-Surface Temperatures on Mercury and the Moon and the Stability of Polar Ice Deposits. *Icarus* 141, 179–193.
- Wechsler, A.E., Simmons, I., 1966. Thermal conductivity and dielectric constant of silicate materials, final report contract NAS8-20076NASA, Washington, D.C.
- Wesselink, A.J., 1948. Heat conductivity and nature of the lunar surface material. *Bull. Astron. Inst. Netherlands* 10, 351–363.
- Wieczorek, M.A., Huang, S., 2006. A Reanalysis of Apollo 15 and 17 Surface and Subsurface Temperature Series. *Lunar Planet. Sci. Conf* 37, 1682.